Propulsion and Energy Forum
July 27-29, 2015, Orlando, FL
51st AIAA/SAE/ASEE Joint Propulsion Conference

Non-Contact Thermal Characterization of NASA's HERMeS Hall Thruster

Wensheng Huang*, Hani Kamhawi†, James L. Myers‡, John T. Yim§
National Aeronautics and Space Administration Glenn Research Center, Cleveland, OH, 44135

and

Gregory Neff**
Western Michigan University, Kalamazoo, MI, 49008

The thermal characterization test of NASA's 12.5-kW Hall Effect Rocket with Magnetic Shielding has been completed. This thruster was developed to support a number of potential Solar Electric Propulsion Technology Demonstration Mission concepts, including the Asteroid Redirect Robotic Mission concept. As a part of the preparation for this characterization test, an infrared-based, non-contact thermal imaging system was developed to measure the temperature of various thruster surfaces that are exposed to high voltage or plasma. An in-situ calibration array was incorporated into the setup to improve the accuracy of the temperature measurement. The key design parameters for the calibration array were determined in a separate pilot test. The raw data from the characterization test was analyzed though further work is needed to obtain accurate anode temperatures. Examination of the front pole and discharge channel temperatures showed that the thruster temperature was driven more by discharge voltage than by discharge power. Operation at lower discharge voltages also yielded more uniform temperature distributions than at higher discharge voltages. When operating at high discharge voltage, increasing the magnetic field strength appeared to have made the thermal loading azimuthally more uniform.

Abbreviations

ARRM	=	Asteroid Redirect Robotic Mission	LEO	=	Low Earth Orbit
GRC	=	Glenn Research Center	SEP	=	Solar Electric Propulsion
GEO	=	Geosynchronous Earth Orbit	STMD	=	Space Technology Mission Directorate
HERMeS	=	Hall Effect Rocket with Magnetic Shielding	TC	=	Thermocouple
			TCT	=	Thermal Characterization Test
IR	=	Infrared	TDM	=	Technology Demonstration Mission
JPL	=	Jet Propulsion Laboratory	TDU	=	Technology Development Unit

I. Introduction

A NASA Glenn Research Center (GRC) and Jet Propulsion Laboratory (JPL) team is developing a 12.5-kW, magnetically shielded Hall thruster under the sponsorship of the NASA Space Technology Mission Directorate (STMD).[1-11] The thruster is named the Hall Effect Rocket with Magnetic Shielding (HERMeS). The development of this thruster is part of an ongoing STMD effort to mature next generation solar electric propulsion systems for use in NASA missions. Various mission concepts that utilize the HERMeS propulsion system have been developed for the Solar Electric Propulsion (SEP) Technology Demonstration Mission (TDM), including the Asteroid Redirect

* Research Engineer, Electric Propulsion Systems, wensheng.huang@nasa.gov, Senior Member.
† Research Engineer, Electric Propulsion Systems, hani.kamhawi-1@nasa.gov, Associate Fellow.
‡ Mechanical Engineer, Thermal Systems, james.l.myers@nasa.gov, Non-Member.
§ Research Engineer, Electric Propulsion Systems, john.t.yim@nasa.gov, Member.
** Graduate Student, Mechanical and Aerospace Engineering, greg.neff@wmich.edu, Member.

Robotic Mission (ARRM).[12] ARRM is a mission concept that involves capturing a piece of a near-Earth asteroid and placing it into a stable lunar orbit where a crewed vehicle will rendezvous with the object.[13] The HERMeS propulsion system also has potential commercial applications for raising the orbit of next generation, higher power communication satellites from low-Earth orbit (LEO) to geosynchronous Earth orbit (GEO).

To meet the requirements of the mission concepts under development, the capabilities of the 12.5-kW HERMeS will be enhanced relative to the current state of the art. Characteristics of the thruster include high system efficiency (≥57%), high specific impulse (3000 s), and high propellant throughput capability (3400 kg). Additionally, HERMeS was designed to deliver similar system efficiency at a more modest specific impulse of 2000 seconds. The 3000-s specific impulse operating point is a trade-off between trip time and propellant load required for high total-impulse mission concepts like ARRM, while the 2000-s operating point is beneficial for time-critical operations like LEO to GEO orbit raising. Furthermore, mission concepts using SEP to transport cargo ahead of a human mission to Mars will benefit from having the mission flexibility to operate over this specific impulse range.

To verify that the 12.5-kW HERMeS meets the established requirements and to reduce several key risks associated with the thruster, a series of tests have been performed on a Technology Development Unit (TDU) thruster. Many of the tests being performed will become references for how to carry out the ground tests of the engineering development unit and qualification tests of the flight unit. As such, these tests both demonstrate the capabilities of the thruster and serve as path-finding activities for future ground and qualification tests. Figure 1 shows a diagram of the testing on HERMeS TDU thus far as well as tests that are planned. Testing that has been completed thus far include the propellant uniformity test[5], magnetic shielding characterization test[11], performance characterization test (PCT)[7], thermal characterization test (TCT), and facility effect characterization test (FECT)[6]. The PCT, TCT, and FECT were performed with a single test setup. The TCT is the main focus of this paper and is highlighted with a red dashed rectangle.

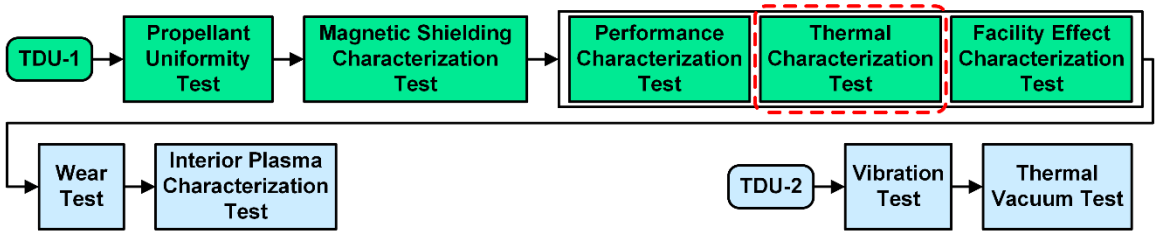

Figure 1. A diagram of the TDU test campaign.

This paper will focus on the development of an infrared (IR) thermal imaging system that was used during the TCT of the TDU1, which was performed at NASA GRC. The remainder of the paper describes the development of the thermal imaging system, test setup, results, analyses, and associated temperature trends.

II. Development of the Thermal Imaging System

One of the earliest example of the use of IR imaging camera to study Hall thruster can be found in the work by Mazouffre, et al., in which the authors studied the SPT100-ML, PPS1350-G, and PPSX000-ML.[14]

Spektor and Beiting were the first to put an IR imaging camera in an environmental enclosure and then put the enclosure in a vacuum chamber.[15] The camera was placed on the thruster firing axis in order to obtain high-resolution images of the front side and discharge channel of the Hall thruster during operation. Note the front side of the thruster is the side with direct line-of-sight to the plasma plume. The thruster team analyzed the test configuration for the 12.5-kW HERMeS and came to the conclusion that placing the IR camera directly downstream of the thruster, as Spektor and Beiting had done, would provide the most accurate and complete thermal measurement of key thruster surfaces where placement of thermocouples (TCs) is impractical. The design of the IR diagnostics system described in this paper was based on the system developed by Spektor and Beiting.[15]

Commercial thermal IR cameras are not normally designed for vacuum operation and also cannot survive the heat load from the impinging plume when placed directly downstream of a Hall thruster. Development of a custom camera was cost prohibitive so the team implemented an environmental enclosure, like the one used by Spektor and Beiting[15], to protect a commercial IR camera. The enclosure is a cylinder with standard flanges attached to each end and is made mostly of stainless steel. Figure 2 shows a cross sectional diagram of the enclosure. The viewing axis of the camera aligns with the cylindrical axis of the enclosure. The front end of the enclosure has a circular uncoated Germanium window attached. No coating was chosen because one side of the window is exposed to high-energy thruster plume ions. Standard feedthroughs were attached to the back end of the enclosure to route IR camera power

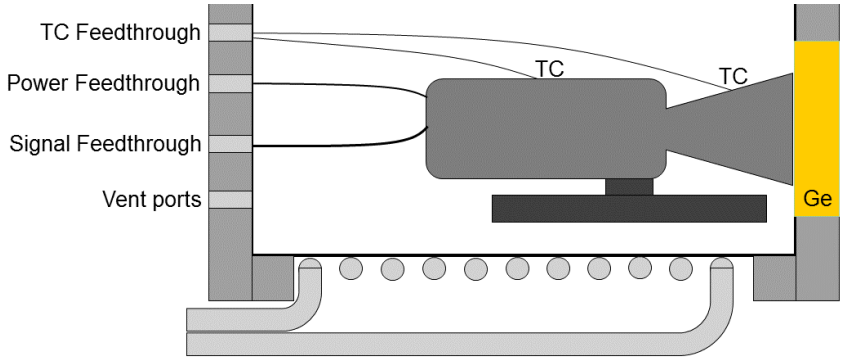

Figure 2. Cross sectional diagram of the environmental enclosure.

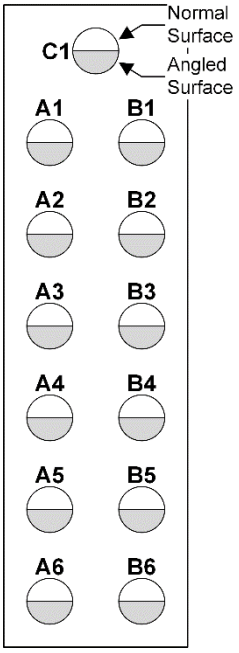

Figure 3. Diagram of the calibration array.

and various signals. The camera is mechanically attached to the endcap with the Germanium window to ensure good alignment between the camera and the enclosure. Wrapped around the exterior of the enclosure is copper tubing through which coolant is continuously pumped. This active cooling keeps the camera temperature within manufacturer specified limits and stabilizes the camera lens against short-term thermal drift that can cause drift in the lens focus. A TC is attached to the camera body to ensure the operating temperature of the camera does not exceed manufacturer specified limits. Another TC is attached to the camera lens. Even with active cooling, long-term thermal drift caused the focal range of the lens to change over time. An automated re-focusing function was implemented in the camera control to compensate for this change. During diagnostic assembly, a pair of vent ports located on the back end of the enclosure was used to perform leak checks. During testing, the ports were sealed with atmospheric pressure air inside the enclosure to promote convective circulation. The ports can alternatively be connected with the exterior of the vacuum facility though this option was not exercised for the TCT.

Since the IR camera must look through a Germanium window, IR light from the thruster undergoes some amount of transmission loss. The transmission loss can change over the course of any test as the surface of the Germanium is ablated by high-energy ions. As such a calibration array was implemented to provide in-situ calibration of the IR emission against an array of known references. The calibration array was made up of a number of boron nitride (BN) samples heated with stainless steel wire heaters and instrumented with TCs. To determine the number of turns of wire to wrap around each sample, a pilot test was performed. The pilot test was performed with two representative BN samples, one wrapped in 5 turns of stainless steel wire and the other wrapped in 10 turns of the same wire. Each sample was instrumented with a type K TC. Both the heaters and the TCs were bonded to the sample using high-temperature ceramic adhesive. The samples were placed inside of a small vacuum chamber and a varying amount of current was supplied to the heaters while the TC signals were recorded. Using the pilot test result, 13 samples spanning operating temperatures of 25-600 °C were made. Figure 3 shows a diagram of the calibration array with the geometric configuration of the samples. Each sample is labeled with a letter and a number. Heaters for samples A1 to A6 were powered by one power supplies while heaters for samples B1 to B6 were powered by a different power supply. Powering the samples with two independent supply was implemented so that the test can continue in the event that one of the power lines failed. C1 has no heater wrapped around it. Each sample has a surface that's normal to the firing axis of the thruster and an angled surface that matches the chamfer angle on the discharge channel of the thruster. The angled surface was implemented in case the emissivity on an angled surface changes differently over time than on a normal surface due, for example, to different backsputter coating rates.

III. Experimental Setup

A. Test Article and Test Matrix

The HERMeS TDU1 was designed to be a 12.5 kW, 3000 s, magnetically-shielded Hall thruster. The thruster had been operated over discharge voltages ranging from 300 to 800 V, corresponding to a specific impulse range of 2000 to 3000 s at full power. The thruster had also been power throttled over discharge powers ranging from 0.6 to 12.5 kW. The cathode mass flow rate was maintained at 7% of the anode mass flow rate. Thruster magnet coils were

energized in such a way that the magnetic shielding topology was always maintained. The only degree of freedom in the magnetic field setting was the strength of the magnetic field. Peak radial magnetic field strength along the discharge channel centerline was chosen as the primary reference point when referring to the strength of the magnetic field. Unless otherwise specified, all references to magnetic field strength of the thruster refers to the peak radial magnetic field strength along the discharge channel centerline.

The TCT had two objectives. The first objective of the TCT was to provide thermal data for validating the thruster thermal model. The thermal model will be used to determine the amount of thermal margin that various thruster components have when the thruster is operated in the space environment. The second objective of the TCT was to find any non-uniformities in the thermal distribution of the thruster that may need to be addressed.

To achieve the objectives of the TCT, the team determined that the thruster should be operated in the most thermally challenging throttle points along with some reference throttle points. Table 1 lists the throttle points for which thermal steady-state was achieved and IR images were captured. Since achieving thermal steady-state took 6-12 hours of continuous operation, only a subset of operating conditions could be tested. All operating conditions were given a label based on discharge voltage and power. The label has the format 'vv-www' where 'vv' is the discharge voltage in volts divided by 10 and 'www' is the discharge power in watts divided by 100. Of the tested steady-state conditions, 30-094, 40-125, and 80-125 are reference throttle points for the thruster. 50-140 is not a reference throttle point but was included to test for any unexpected thruster behavior should the upper power limit of 12.5 kW be exceeded during on-orbit operation. Magnetic field strength was set to provide the best thruster efficiency while having a reasonable amount of margin (>25 gauss) against oscillation mode transitions. The only exception is 80-125B, where the magnetic field strength was set to the maximum design value for HERMeS to test how much thermal margin is available in the event that the maximum magnetic field is needed for on-orbit operation. The magnetic field strength for 80-125B is about twice as high as the magnetic field strength for 80-125.

Table 1. List of thruster operation conditions.

Label	Discharge voltage, V	Discharge power, kW	Magnetic field strength
30-094	**300**	**9.4**	**Nominal**
40-125	**400**	**12.5**	**Nominal**
50-140	**500**	**14.0**	**Nominal**
80-125	**800**	**12.5**	**Nominal**
80-125B	**800**	**12.5**	**Max**

B. Test Facility and Diagnostic

Testing was conducted in NASA GRC's vacuum facility 5 (VF5). This cylindrical facility is 4.6 m in diameter, 18.3 m long, and is equipped with cryo-panels and 20 oil diffusion pumps. Only the cryo-panels were in use for this test. The thruster was mounted on a thrust stand located close to the bulk of the cryo-panels firing toward a graphite-lined end-cap. Facility pressures were monitored with four ion gauges, three of which were mounted next to the thrust stand and were calibrated for xenon. The fourth ion gauge was mounted on the facility wall near the axial center of the chamber and was calibrated for air. During testing, the xenon pressure by the thruster varied from 3.8×10^{-6} to 6.7×10^{-6} Torr.

The calibration array was located to one side of the thruster with the downstream surface of the array slightly upstream of the thruster radiator. The IR camera was located 5.9 m downstream of the thruster exit plane, on the firing axis of the thruster, but was tilted slightly so that its viewing cone covers the calibration array as well as the bulk of the thruster. Figure 4 shows a picture of the test setup. A mirror for high-speed imaging from the facility effect characterization test was present but was out of the line of sight of the IR camera. Although not visible in the figure, a shutter had been mounted to protect the IR camera Germanium window when the camera was not in use. Figure 5 shows a close-up picture of the calibration array after testing was completed. In this picture, the array could be seen situated just to the right of the thruster radiator. The 'A' bank of the array was typically operated at 2.5 A of heater current while the 'B' bank was operated at 1.0 A.

Data from both the IR camera and the calibration array TCs were recorded on a single computer, which was operating a custom data recording program. The custom program also handled periodic re-focusing of the camera to keep the thruster in focus.

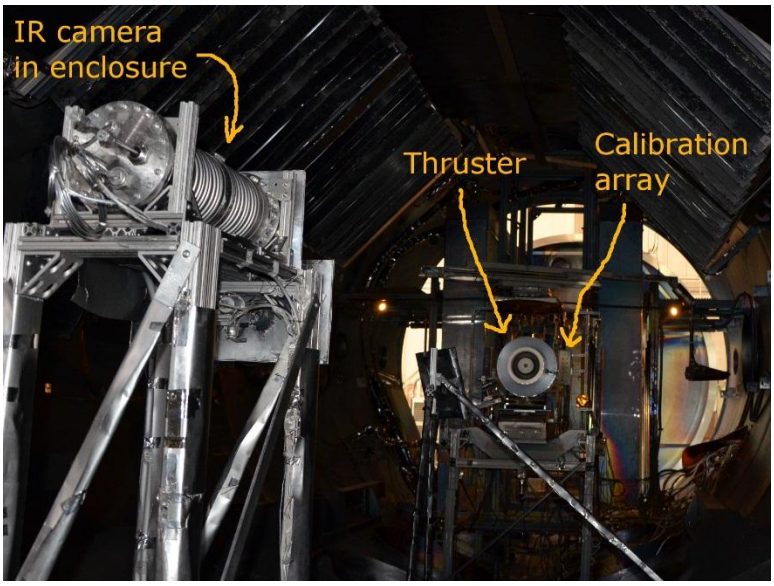

Figure 4. Picture of the experimental setup.

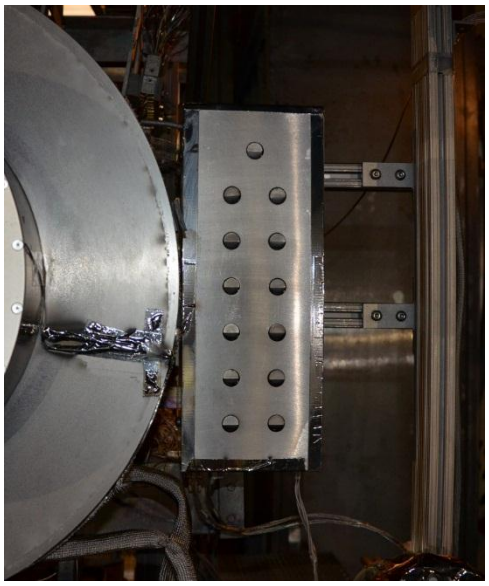

Figure 5. Close-up picture of the calibration array after testing was completed.

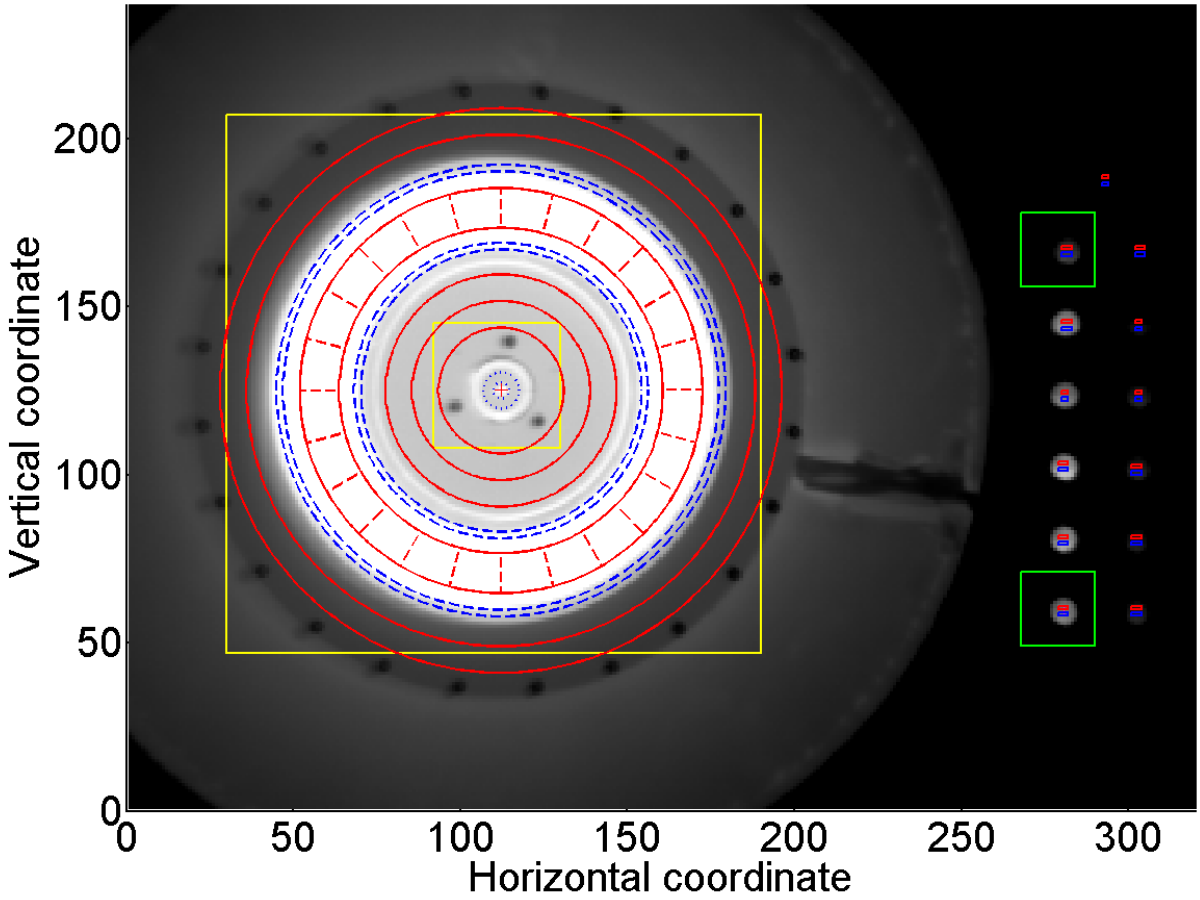

Figure 6. Sample IR camera image with boundaries of the analysis regions overlaid.

IV. Data Analysis

A. Thermal Image Analysis and Correction Factors

Data from the IR camera were stored in the form of 2D images where the value of each cell was proportional to the measured radiance. The first step in the data analysis process was to extract the radiance from various regions on the thruster and the calibration array. Figure 6 shows an image of how the analysis program divides up a particular IR camera image into regions. The horizontal and vertical axis show the pixel counts. To start with, the program searched between the two yellow squares to find the brightest pixels that corresponded to the anode of the thruster. The program then performed a circle fit to identify the center of the thruster. At the same time, the program found the center of the calibration samples A1 and A6. The distance between A1 and A6 was used to determine the scale of the image. This step was found to be necessary because as the temperature distribution on the IR camera lens drifted over the course of the test, the magnification on the image also drifted.

Having identified the thruster center and the image scale, the program divided the thruster up into multiple concentric layers. In order from the innermost to outermost, the layers were inner front pole 1, inner front pole 2, inner chamfer of the discharge channel, anode, outer chamfer of the discharge channel, and outer front pole. The inner front pole was divided into two layers to determine whether any radial non-uniformity existed. Temperatures in the inner front pole 2 layer turned out to always be within 0 to +10 °C of the temperatures in the inner front pole 1 layer at the same azimuthal angle. This difference was considered within the measurement uncertainty of the IR camera so inner front pole temperatures reported in this paper are the average of inner front pole 1 and 2. Each layer was further divided into 24 azimuthal slices to help identify any azimuthal non-uniformity in the thruster temperature distribution. Each of the 13 calibration samples are also located. For each sample two rectangular regions were partitioned, one over the normal surface and another over the angled surface. For each region partitioned by the program a single radiance value is calculated by averaging over the region.

For the second step in the data analysis process, the radiance data and the temperature data from the calibration samples were used to generate two calibration curves per image. One curve was used for normal surfaces while the other was used for angled surfaces, which were the BN chamfer regions. Interestingly, although A6 was designed to be the hottest sample in the array, A4 were often hotter. This phenomenon was most likely caused by heat radiated from the sides of the calibration sample being trapped inside the calibration array case, which caused the middle part of the case to become hotter than the ends. While the heating of the case meant that the samples did not operate at their intended temperatures, the samples still had a sufficient spread in temperatures to provide a good calibration curve. A side effect of the case heating was that the unheated sample, C1, was typically at 200 °C. The samples also appeared to become slightly hotter when the thruster operated at higher temperatures.

Preliminary analysis showed that a surface within the channel, specifically the anode, also reflected some of the IR emission from other surfaces within its view. As a result, the absolute value of the anode temperature was likely overestimated. This issue will be corrected in future work and only azimuthal variation in anode temperature will be presented in this paper. Another potential issue was differences in emissivity between some thruster components and the calibration samples. The anode downstream surface was grid-blasted to increase its emissivity. However, since only azimuthal variations of the anode will be looked at, no emissivity correction was applied for the anode. The inner and outer front poles were both spray-coated with aluminum oxide. The discharge channel and the calibration samples were made of boron nitride. However, by the time the IR images were taken the thruster had been operated long enough for a backsputter-deposited coating of varying thickness to form over all downstream facing thruster components. Since the facility was covered in graphite, the backsputter-deposited coating should be nearly pure carbon. Thus, each region measured by the IR camera has an emissivity somewhere between that of the original material and graphite. Since IR camera images were taken well into the test campaign, analysis was carried out with the assumption that surfaces were sufficiently coated to have emissivity similar to sputter-coated BN. Using an IR reflectometer, the team measured the emissivity of a number of clean and sputter-coated BN samples. The measured emissivity varied from 0.83 to 0.85 for all samples. For this study, no correction for emissivity was made, though the variation in emissivity was used in the uncertainty analysis. Note that emissivity of materials can change with temperature but no literature is available on how the emissivity of BN and aluminum oxide coated metal varies. A study is currently being performed to determine these relationships and any potential correction is left for future work.

B. Uncertainty Analysis

There were a number of uncertainty sources affecting the IR camera temperature measurement. The most important sources of uncertainties include variation in emissivity of surfaces as compared with the calibration samples and finite reflectivity of regions that have high temperature component within their view. Finite reflectivity

effects will be treated in future work. Uncertainty associated with changing emissivity affects different regions differently. Since the BN discharge channel and the calibration samples were made of the same material and were coated by backsputtered material at similar rates, the difference in emissivity between them were expected to be very small. This difference was estimated to be within 0.01. On the other hand, the emissivity of the front poles was likely not as similar to sputter-coated BN compared to the sputter-coated discharge channel. The uncertainty in the front pole emissivity was estimated to be ±0.025. For the radiance measured during the TCT, the uncertainty on temperature due to variations in emissivity was estimated at ±25 °C for the discharge channel regions and ±50 °C for the front pole regions.

V. Results and Discussions

Figures 7 to 11 show the processed IR camera images for the operating conditions 30-094, 40-125, 50-140, 80-125, and 80-125B, respectively.

Table 2 summarizes the average and azimuthal peak-to-peak in temperatures for the various locations and operating conditions as measured by the IR camera. Note that no average values were reported for anode temperature because further work is needed to account for the effect of finite reflectivity. From Table 2 and Figs. 7 to 11, the component temperatures on the HERMeS thruster appeared to be driven by both the discharge voltage and discharge power, as opposed to only the discharge power. This trend was most obvious in that the component temperatures are slightly lower for the 500 V, 14 kW condition than for the 800 V, 12.5 kW condition. The thruster also appeared to be very uniform in temperature when operating at low discharge voltage but showed some azimuthal non-uniformity when operating at high discharge voltage. In particular, at 800 V, 12.5 kW, nominal magnetic field strength, there was a clear azimuthal variation in temperature on the anode. The radiance at the 8 to 11 o'clock position on the anode was quite a bit higher than at the 2 to 5 o'clock position. Comparing the two 800 V cases (Figs. 10 and 11), one can see that the anode exhibited similar azimuthal non-uniformity patterns but the high magnetic field strength case showed a lower peak-to-peak variation in radiance. This phenomenon suggests that operating at higher magnetic field strength may help even out the heat loads on the thruster. At the same time, operating at higher magnetic field strength appeared to drive up component temperatures, especially the inner front pole and the inner chamfer on the discharge channel. This trend was driven at least partially by increased self-heating of the magnet coils.

Table 2. Summary of temperatures measured by the IR camera.

*pk-pk refers to azimuthal peak-to-peak values.

	30-094		40-125		50-140		80-125		80-125B	
	Avg.	pk-pk	Avg.	pk-pk	Avg.	pk-pk	Avg.	pk-pk	Avg.	pk-pk
Anode, radiance, %		12%		9.5%		17%		35%		18%
Inner front pole, °C	355	6	459	6	539	14	567	20	623	15
Outer front pole, °C	252	30	358	12	359	17	354	24	377	15
Inner chamfer, °C	362	19	496	26	545	39	538	90	645	102
Outer chamfer, °C	349	34	494	32	553	85	580	213	608	71

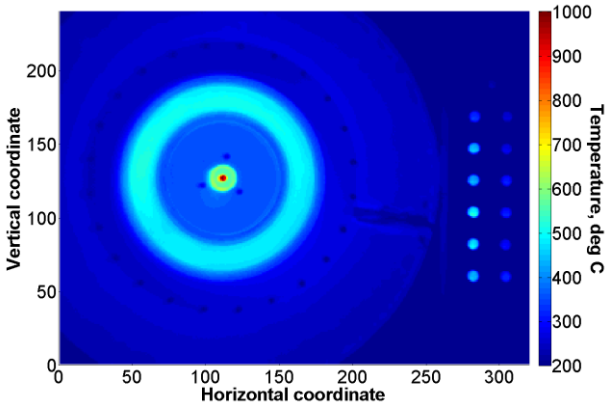

Figure 7. Processed IR camera image for 300 V, 9.4 kW operation.

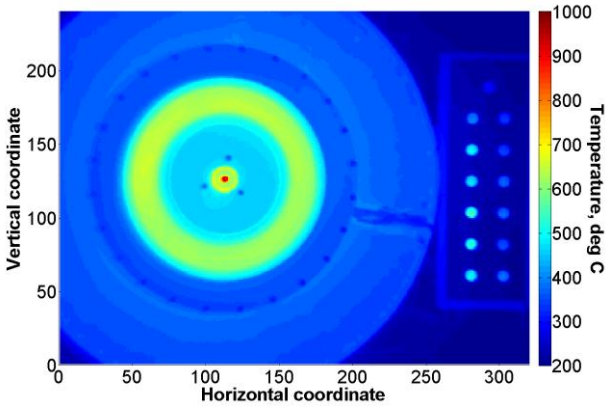

Figure 8. Processed IR camera image for 400 V, 12.5 kW operation.

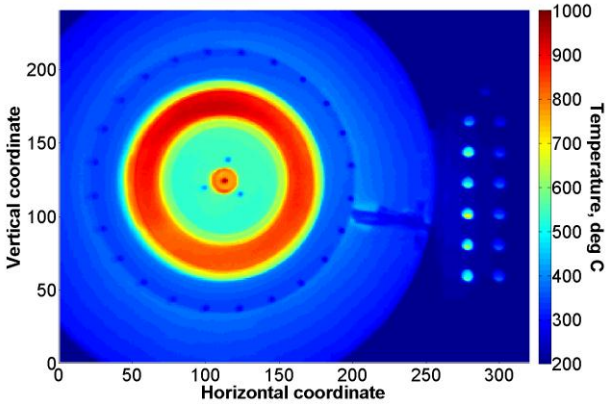

Figure 9. Processed IR camera image for 500 V, 14 kW operation.

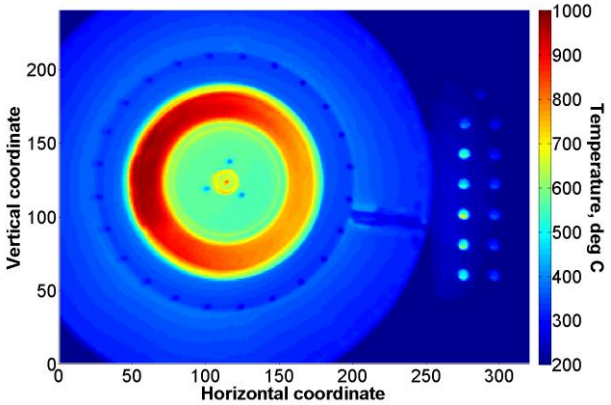

Figure 10. Processed IR camera image for 800 V, 12.5 kW operation with nominal magnetic field strength.

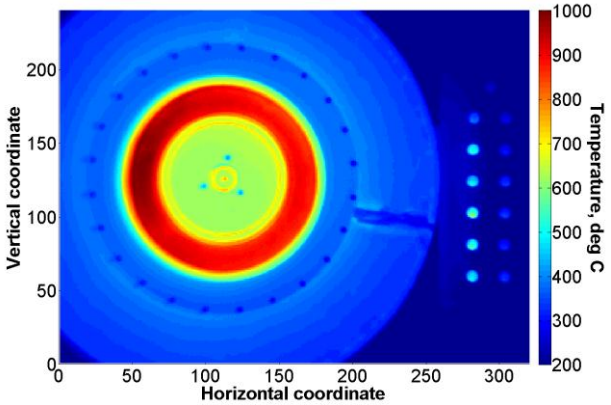

Figure 11. Processed IR camera image for 800 V, 12.5 kW operation with high magnetic field strength.

Note that the peak-to-peak temperature of 213 °C on the outer chamfer for 800 V, 12.5 kW operation may be a camera artifact. A close examination of Fig. 10 shows that the left side of the image is slightly fuzzy. The fuzziness appears to be due to a ghost image superimposed on top of the original image. A ghost image can form as a result of secondary reflection on optics that do not have anti-reflect coatings, as was the case with the Germanium window. Towards the center of the image, the ghost image should overlap with the original. However, towards the edges, the overlap is not perfect. Since the chamfer region was very thin from the perspective of the IR camera, it is possible that the ghost image from the nearby anode region caused an artificial increase in measured radiance at the 9 o'clock outer chamfer position. Figure 12 shows the inner and outer chamfer temperatures plotted against the azimuthal angle for the 800 V operating conditions. Azimuthal angle is 0 degrees at the top of the thruster and increases when traveling clockwise while viewing the thruster. This figure shows a clear jump in outer chamfer temperature at the 9 o'clock position (azimuthal angle of 270°) for the nominal magnetic field strength case that was not present in other instances. Assuming this jump in temperature was an artifact, the actual peak-to-peak temperature for the outer chamfer when the thruster was operating at 800 V, 12.5 kW, nominal magnetic field strength, was ~100 °C.

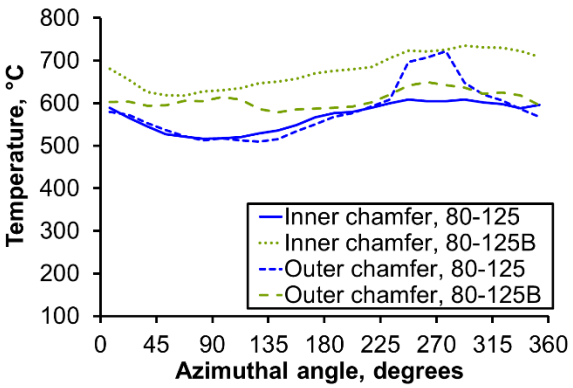

Figure 12. Chamfer temperatures versus azimuthal angle for the 800 V operating conditions.

VI. Conclusions

The thermal characterization test of NASA's 12.5-kW Hall Effect Rocket with Magnetic Shielding had been completed and a non-contact thermal imaging system was successfully deployed during the test. To obtain the most accurate measurement possible, an in-situ calibration array was also successfully deployed.

Examination of the front pole and discharge channel temperatures showed a number of interesting trends. One, the thruster temperature appeared to be driven by both the discharge voltage and discharge power. Two, operation at lower discharge voltages (300-500 V) yielded more uniform temperature distributions than at higher discharge voltages (800 V). Three, when operating at high discharge voltage, increasing the magnetic field strength appeared to have made the thermal loading azimuthally more uniform.

The tests also revealed a few issues that require future work. Foremost amongst these issues was the need to account for finite reflectivity so that accurate anode temperatures can be obtained. Another issue was the presence of ghosting effects that may need to be accounted for in future analysis. A third issue was the uncertainties in the emissivity of materials that drove up the uncertainties in the front pole temperatures. These issues are currently being examined and will be resolved in future work.

Acknowledgments

We thank the NASA Space Technology Mission Directorate Solar Electric Propulsion Technology Demonstration Mission project for funding this work, and Daniel A. Herman and Richard R. Hofer for managing the work. And we thank Kevin L. Blake, George P. Jacynycz, Thomas A. Ralys, and Terrell J. Jensen for the fabrication, assembly of the test setup, and operation of the vacuum facility. We also thank Rostislav Spektor and Edward J. Beiting for fruitful discussions.

References

[1]Kamhawi, H., et al., "Overview of the Development of the Solar Electric Propulsion Technology Demonstration Mission 12.5-kW Hall Thruster", *50th AIAA/ASME/SAE/ASEE Joint Propulsion Conference*, AIAA-2014-3898, doi:10.2514/6.2014-3898, Cleveland, OH, Jul 28-30, 2014.

[2]Herman, D. A., et al., "The Development of the Ion Propulsion System for the Solar Electric Propulsion Technology Demonstration Mission", *34th International Electric Propulsion Conference*, 2015-008, Kobe, Japan, Jul 4-10, 2015.

[3]Hofer, R. R., et al., "Development Approach and Status of the 12.5 kW HERMeS Hall Thruster for the Solar Electric Propulsion Technology Demonstration Mission", *34th International Electric Propulsion Conference*, 2015-186, Kobe, Japan, Jul 4-10, 2015.

[4]Hofer, R. R., et al., "Design Methodology and Scaling of the 12.5 kW HERMeS Hall Thruster for the Solar Electric Propulsion Technology Demonstration Mission", *62nd Joint Army-Navy-NASA-Air Force Propulsion Meeting*, JANNAF-2015-3946, Nashville, TN, Jun 1-4, 2015.

[5]Huang, W., Yim, J. T., and Kamhawi, H., "Design and Empirical Assessment of the HERMeS Hall Thruster Propellant Manifold", *62nd Joint Army-Navy-NASA-Air Force Propulsion Meeting*, JANNAF-2015-3926, Nashville, TN, Jun 1-4, 2015.

[6]Kamhawi, H., Haag, T., Huang, W., and Hofer, R. R., "The Voltage-Current Characteristics of the 12.5 kW Hall Effect Rocket with Magnetic Shielding at Different Background Pressure Conditions", *62nd Joint Army-Navy-NASA-Air Force Propulsion Meeting*, Nashville, TN, Jun 1-4, 2015.

[7]Kamhawi, H., et al., "Performance Characterization of the Solar Electric Propulsion Technology Demonstration Mission 12.5-kW Hall Thruster", *34th International Electric Propulsion Conference*, 2015-007, Kobe, Japan, Jul 4-10, 2015.

[8]Yim, J. T. and Huang, W., "Flow Analysis and Modeling of the HERMeS Hall Thruster Propellant Manifold", *62nd Joint Army-Navy-NASA-Air Force Propulsion Meeting*, JANNAF-2015-3884, Nashville, TN, Jun 1-4, 2015.

[9]Lopez Ortega, A., Mikellides, I. G., and Katz, I., "Hall2De Numerical Simulations for the Assessment of Pole Erosion in a Magnetically Shielded Hall Thruster", *34th International Electric Propulsion Conference*, 2015-249, Kobe, Japan, Jul 4-10, 2015.

[10]Mikellides, I. G., et al., "Hall2de Simulations of a 12.5-kW Magnetically Shielded Hall Thruster for the NASA Solar Electric Propulsion Technology Demonstration Mission", *34th International Electric Propulsion Conference*, 2015-254, Kobe, Japan, Jul 4-10, 2015.

[11]Shastry, R., Huang, W., and Kamhawi, H., "Near-Surface Plasma Characterization of the 12.5-kW NASA TDU1 Hall Thruster", *51st AIAA/ASME/SAE/ASEE Joint Propulsion Conference*, Orlando, FL, Jul 26-30, 2015.

[12]Manzella, D. and Hack, K., "High-Power Solar Electric Propulsion for Future NASA Missions", *50th AIAA/ASME/SAE/ASEE Joint Propulsion Conference*, AIAA-2014-3718, doi:10.2514/6.2014-3718, Cleveland, OH, Jul 28-30, 2014.

[13]Brophy, J. R. and Muirhead, B., "Near-Earth Asteroid Retrieval Mission (ARM) Study", *33rd International Electric Propulsion Conference*, 2013-082, Washington, DC, Oct 6-10, 2013.

[14]Mazouffre, S., Echegut, P., and Dudeck, M., "A calibrated infrared imaging study on the steady state thermal behavior of Hall effect thrusters", *Plasma Sources Science and Technology*, Vol. 16, No. 1, doi:10.1088/0963-0252/16/1/003, Feb, 2007, pp. 13-22.

[15]Spektor, R., et al., "Infrared Thermographic Diagnostic for Imaging Hall Thrusters", *33rd International Electric Propulsion Conference*, 2013-452, Washington, DC, Oct 6-10, 2013.